Research Article Vol. 29, No. 2 / 18 January 2021 / Optics Express 719
Optics EXPRESS

FPGA-based digital chaotic anti-interference lidar system

LIYAN FENG,[1] HUAZHENG GAO,[2] JIANXUN ZHANG,[2] MINGHAI YU,[2] XIANFENG CHEN,[1,3] WEISHENG HU,[2] AND LILIN YI[2,*]

[1]State Key Lab of Advanced Optical Communication Systems and Networks, School of Physics and Astronomy, Shanghai Jiao Tong University, Shanghai 200240, China
[2]State Key Lab of Advanced Optical Communication Systems and Networks, School of Electronic Information and Electrical Engineering, Shanghai Jiao Tong University, Shanghai 200240, China
[3]Collaborative Innovation Center of Light Manipulation and Applications, Shandong Normal University, Jinan 250358, China
*lilinyi@sjtu.edu.cn

Abstract: We use the chaotic signal generated by a field-programmable gate array (FPGA) to establish a digital chaotic pulse lidar system, which can achieve mid-range detection and high ranging accuracy without a complex optical structure. We employ the FPGA to generate random sequences with different modulation rates based on different chaotic iterative equations and initial values. By selecting the initial value and improved logistic equations, we successfully achieve centimeter-level ranging accuracy. Experiments have proved that the digital chaotic lidar system can effectively resist the interference of chaotic signals, square wave signals, and sine wave signals with modulation frequencies of 10 MHz, 100 MHz, 200 MHz, and 1 GHz, showing its strong anti-interference capability.

1. Introduction

Light detection and ranging (lidar), benefitting from the merits of high accuracy and precision, long-distance active imaging system, and high imaging speed and resolution, has been widely applied in unmanned aerial vehicles, medical imaging, nondestructive examination, and remote sensing in recent years [1–4]. According to the modulation mode of the laser, lidar systems can be divided into pulsed lidar and continuous wave (CW) lidar systems. For conventional pulsed lidar systems, the range of the target can be determined by the time-of-flight (TOF) of the emitted repetitive short pulses [5,6]. However, it is vulnerable to interference and attack from malicious hackers using the intercepted repetitive pulses [7,8].

To prevent the interference problem, new types of pulsed lidar systems, such as the chaotic pulse position modulation (CPPM) and the photon-driven stochastic pulse position modulation (SPPM) have been studied [9–11]. However, the rate of the PPM is not high due to the current technical limitations. Therefore, PPM requires multiple calculations and takes long calculation time, which is more suitable for remote fixed object measurement. In addition, modulated CW lidar systems with excellent anti-interference performance become the focus of research in the field of lidars, such as coherent ranging, optical chaotic and pseudorandom-modulation lidar systems. Coherent ranging, also known as frequency-modulated continuous-wave (FMCW) laser-based lidar maps distance to frequency using frequency-chirped waveforms and prevents interference from sunlight and other lidar systems [12–14]. However, this technology requires precisely chirped and highly coherent laser sources and is expensive to develop, hindering widespread use of the lidar system. Therefore, with low cost, high-precision measurement, and anti-interference capability, chaotic lidars based on indirect time-of-flight (iTOF) receive more attentions, where the ranging information is achieved by calculating the cross-correlation of the transmitted and received chaotic waveforms [15]. Compared with the pseudo-random data, the

#414185 https://doi.org/10.1364/OE.414185
Journal © 2021 Received 6 Nov 2020; revised 11 Dec 2020; accepted 17 Dec 2020; published 4 Jan 2021

Optics EXPRESS

chaotic waveforms have no periodicity and are difficult to be predicted, therefore the chaotic lidars show better anti-interference performance than pseudorandom-modulation lidar systems.

The optical chaotic lidar was first proposed and verified by Myneni *et al*. with the chaotic semiconductor laser achieving high-precision ranging in 2001 [16]. Furthermore, the multi-target ranging chaotic lidar, the noise suppression of the chaotic lidar, and the synchronized chaotic lidar systems were proposed subsequently [17–20]. Recently, a new type of 3D pulse chaotic lidar system was proposed, which uses delayed zero beat and time gating to generate pulse homodyne chaos and improve energy utilization [21]. Although the bandwidth of the optical chaotic signal can be easily achieved on the GHz level to obtain the accuracy and resolution of millimeter level, the optical chaotic system requires a complicated internal optical system with high system cost which limits its practical applications. Besides, the high accuracy not only relies on the bandwidth of optical chaotic laser, but also the receiving devices. If the bandwidth of the receiving devices is limited, the high bandwidth of the transmitting signal is not indispensable. By contrast, the random sequence generated by the digital chaos equation is easy to implement by hardware with low cost, which has been a good source candidate for radio detection and ranging systems [22,23]. While, the experimental exploration and the anti-interference performance of the digital chaotic lidar based on the chaos equation has not yet been reported.

In this study, we utilized the anti-interference ability of chaotic signals and built a digital chaotic anti-interference lidar system based on field-programmable gate array (FPGA) to solve the problems of complex optical chaotic system structure and single modulation mode. Based on random chaotic binary signals, the system can achieve effective anti-interference performance under the jamming of chaotic signals, square wave signals, and sine wave signals with modulation frequencies of 10 MHz, 100 MHz, 200 MHz, and 1 GHz, while maintaining long-distance detection of 14 m and high ranging accuracy of 8 cm. With FPGA, we can generate random sequences with various modulation rates according to different chaotic iteration equations and initial values. The initial values of 0.7 and improved logistic equations are selected through simulation to successfully achieve millimeter-level ranging accuracy in the best case. Moreover, we quantitatively analyzed system factors such as peak side-lobe level (PSL), ranging accuracy, modulation rate, and code lengths of the digital chaotic lidar system.

2. Setup of the digital chaotic lidar system

The schematic setup of the digital pulse chaotic lidar system is shown in Fig. 1. The system includes the digital chaotic light source, the transmitting and receiving optical system, and the signal acquisition and processing module. The digital chaotic signal used to modulate the directly modulated laser (DML, Xeston XGT8011-001D) can be generated by an arbitrary waveform generator (AWG, Tektronix AWG7122C) or FPGA (Stratix V 5SGXEA7K2F40C2). Considering the convenience of practical commercial systems, we use the signal generated by FPGA as the signal source for the ranging experiment. However, AWG can generate arbitrary digital modulation signals within 12 GHz bandwidth, so when testing the ranging characteristics under interference, we use the signal generated by the AWG as the interference signal source, and the signal generated by the FPGA as the lidar signal source. The wavelength of the DML is 1550 nm and the optical power is 10 dBm. The voltage of the modulating signal is 1 V. A detailed analysis of the modulating signal will be introduced in the next section.

Due to the requirements of the subsequent cross-correlation calculation, the signal source output is split into two channels, one serving as the reference signal input to the oscilloscope (Infiniium DSO9254A) and the other as the probe signal to modulate the DML. The delay of their internal circuit can be processed uniformly through the calibration distance of the ranging. For the requirement of long-distance measurement, an erbium-doped fiber amplifier (EDFA) is used to amplify the optical signal. Considering that we only preliminary verify the feasibility of

Optics EXPRESS

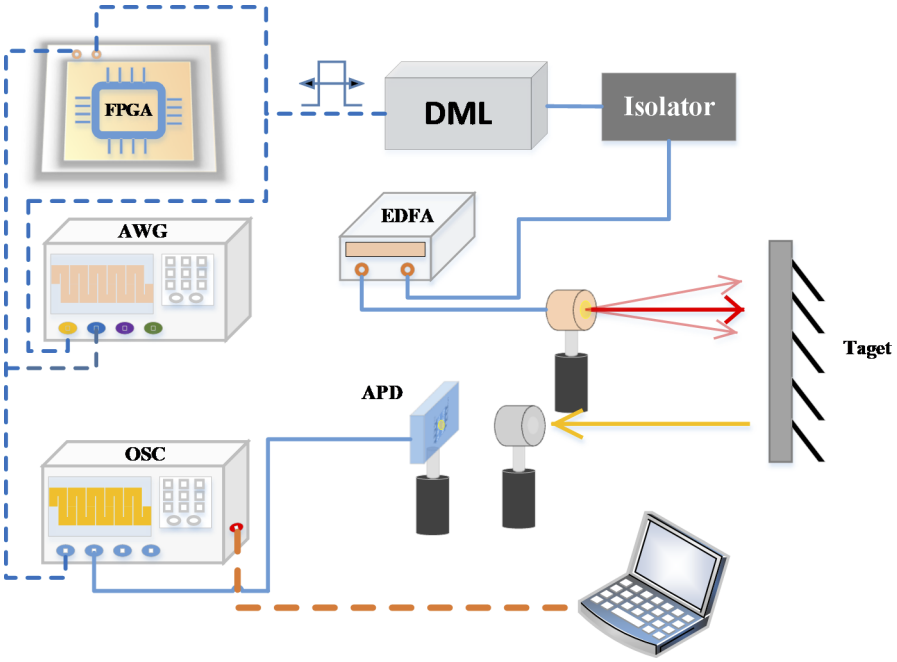

Fig. 1. Schematic setup of the digital chaotic anti-interference lidar system. DML: directly modulated laser; AWG: arbitrary waveform generator; APD: avalanched photodetector; EDFA: erbium-doped fiber amplifier; OSC: oscilloscope.

this scheme and study the characteristics of the system, the launched laser power is amplified to 200 mW.

The transmitted laser beam output by the fiber of the EDFA is emitted into space through the collimator with a spot diameter of about 2.8 mm and a full divergence angle of about 0.69 mrad. The target for distance measurement is a standard plate with a reflectivity of 60%. The echo signal backscattered from the target is collected by a receiving lens with a focal length of 100 mm and a field of view of about 84.3 mrad, which is detected and received by the avalanched photodetector (APD, 200 MHz). After the detector converts the optical signal into an electrical signal, we perform cross-correlation calculations between the echo signal and the local reference signal. The distance information of the target is obtained from the peak value of the cross-correlation curve, and then the anti-interference characteristics of the system are further analyzed.

3. Signal source generated by chaotic maps

For the traditional pseudo-random code, the m sequence as a representative can be generated by an n-stage linear shift register and the longest possible period of the sequence is $2^n - 1$. However, the disadvantage of this sequence is that the number of registers is limited, resulting in the sequence being periodic and easy to be attacked. By contrast, aperiodic digital chaotic coding sequence generated by FPGA with random initial values can prevent the problem of the complex optical structure requirement and single modulation mode of optical chaotic systems while maintaining high resolution and the effectiveness of anti-malicious attacks. To achieve the best chaotic maps, simulation results are presented in this section. Four kinds of primary digital chaotic sequences with arbitrary lengths are generated from chaotic maps of Chebyshev, Logistic, improved Logistic, and Tent with random initial values. For the anti-interference coding sequence, it is necessary to select a sequence with a high autocorrelation coefficient, a small

Optics EXPRESS

autocorrelation sidelobe, a small cross-correlation coefficient, a sufficient code sequence, and as much complexity as possible. The autocorrelation curves of these four sequences are shown in Fig. 2. The sidelobe level of the Tent sequences is relatively higher while the other three sequences have no significant difference from each other. Considering the complexity of FPGA implementation, we choose the improved logistic sequence as the chaotic coding sequence, which requires fewer logical resources. It is very convenient to generate a chaotic spread spectrum sequence from the improved Logistic map by giving an iterative formula and initial value of a chaotic equation.

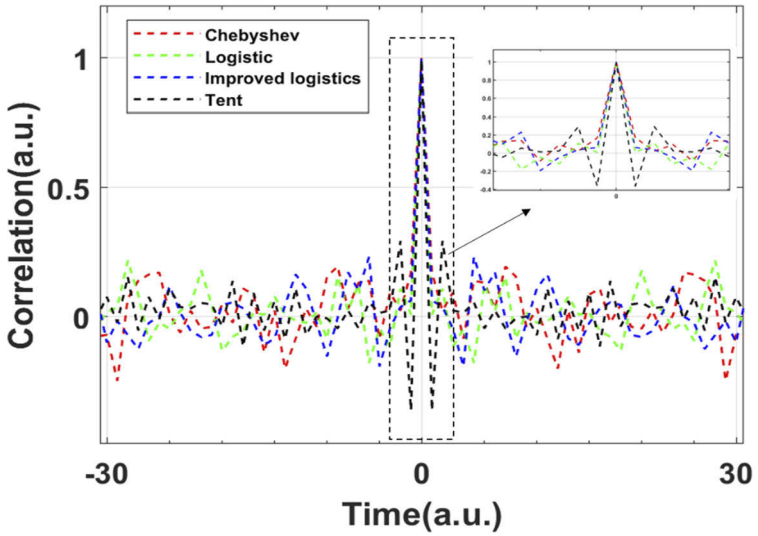

Fig. 2. The autocorrelation curves of Tent sequence, Chebyshev sequence, Logistic sequence, and improved Logistic sequence.

In order to facilitate the subsequent digitization processing, the Logistic mapping is usually improved, that is, its mean value becomes zero. The improved Logistic mapping is

$$X_{n+1} = f(X_n) = 1 - 2(X_n)^2, \quad -1 < X_{n+1} < 1, \tag{1}$$

which is a special case of logistic mapping and can be obtained by simple derivation. The probability density function of this mapping is

$$p(x) = \begin{cases} \frac{1}{\pi\sqrt{1-x^2}}, & -1<x<1 \\ 0, & \text{otherwise} \end{cases} \tag{2}$$

The mean value of the improved Logistic mapping is $\bar{x} - \lim_{N\to\infty} \frac{1}{N} \sum_{i=0}^{N-1} x_i = 0$.

Due to the sensitivity of the initial value of the chaotic equation, the PSLs with different correlation symbol lengths can be calculated to quantify the differences of the initial value to optimize the correlation performance. PSL, which is defined as the ratio of the maximum sidelobe to the peak, is associated with the probability of a false signal and the ranging accuracy in the subsequent ranging experiments [17].

$$PSL = 10\log\left(\frac{\max(P_s)}{P}\right) \text{ [dB]}, \tag{3}$$

where P_s is the sidelobe value of the correlation curve, and P is the peak value. As shown in Fig. 3(a), the PSLs of the autocorrelation traces of the improved Logistic chaotic signal with three

Optics EXPRESS

randomly selected initial values are plotted as the function of the correlation symbol lengths. The solid lines are the fitted regressions and X_1 is the initial value. It can be seen that the longer the correlation code length is, the better the PSL effect is. While, considering the practical implementation, the computation time can be effectively shortened by reducing the correlation length. Therefore, through comprehensive consideration of the above two factors, the correlation symbol length calculated in the subsequent ranging experiments $L = 80$ is used. As we can see, within 850 symbol lengths, the PSL with an initial value of 0.7 performs better and more stable than that of 0.32 and 0.1. When the correlation symbol length is 80, the variation of PSL with the initial value X_1 is shown in Fig. 3(b). It can be seen that different initial values have different effects on the correlation of the pulse sequence, and there is no obvious regularity. However, there is little difference in the correlation performance of different initial values. In order to further reduce the crosstalk between lidar systems, different initial values can be selected between different digital chaotic lidars. In addition, we found that while keeping other factors constant, the autocorrelation results of data in different time intervals will also have subtle differences. Therefore, the selection of the initial value will have an optimal solution only under special circumstances. However, in practical applications, the data used for correlation calculations is disordered and constantly refreshed. Thus, the initial value can be set within a reasonable range ($0<X_1<0.5$, $0.5<X_1<1$). While, in the subsequent experiments, considering the correlation symbol length ($L = 80$) we used, the PSL performs better and more stable and remains below −6 dB when the initial value is 0.7. Therefore, the initial value of the equation we adopted in subsequent experiments is set at 0.7.

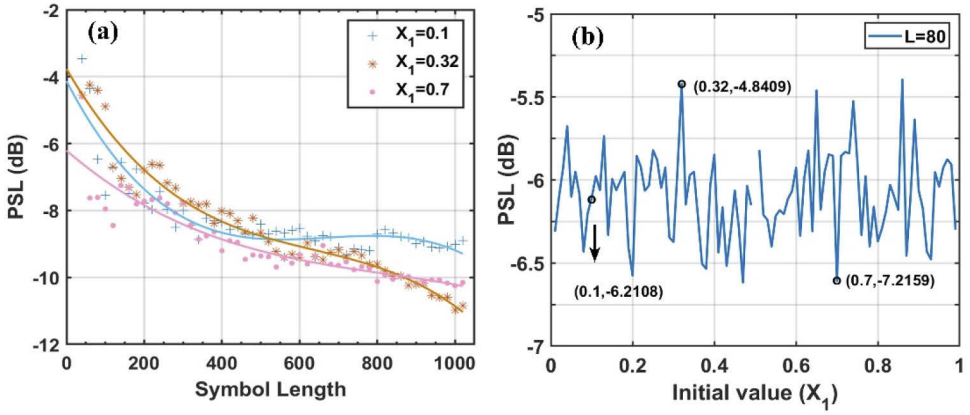

Fig. 3. (a) The influence of initial value on PSL with different symbol lengths. (b) The variation of PSL with the initial value X_1.

Furthermore, on the basis of optimized parameters, the chaotic system is designed by DSP Builder according to the improved logistic iterative equation. As shown in Fig. 4(a), the model is converted into a VHDL file through Signal Compiler to generate a Quartus II project file, which is downloaded to the FPGA for generating the chaotic signals in real time. Since the equation parameters are all set to signed numbers, a comparator is added after the equation model to obtain the binary chaotic signal. The threshold is set to 0 to obtain the simulation waveform as shown in Fig. 4(b), and its autocorrelation curve is shown in Fig. 4(c), which has a delta function-like trace to achieve precise detection without range ambiguity expectedly.

Optics EXPRESS

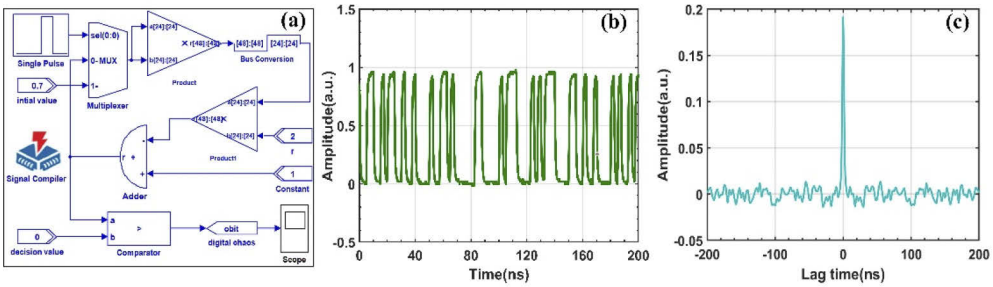

Fig. 4. (a) The model principle to generate the digital pulse chaotic signal. (b) The time series and (c) autocorrelation of the transmitted waveform.

4. Experimental result

4.1. Ranging experiment

Based on the above ranging system, we performed static tests by varying the distance (2–14 m) between the receiving APD and a targeted panel (60% reflectivity) in the laboratory. To further demonstrating the performance of ranging, we measured the distance every 25 cm using our chaotic lidar ranging system. Figure 5 shows the measured distance (blue spot) and corresponding accuracy (red) computed as the difference between true (solid black) and measured distance obtained at different ranges. As can be seen, the accuracy of distance measurement can achieve 0.2 cm in the best case. While in the worst situation, the accuracy of 8.2 cm is achieved and the average accuracy is 4.22 cm.

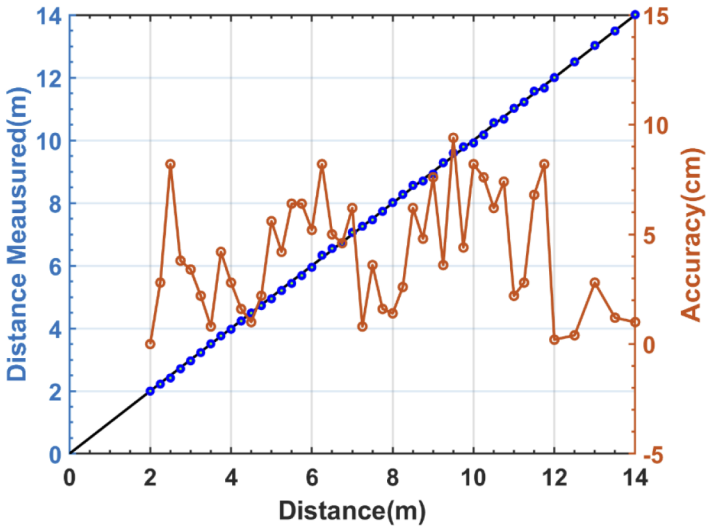

Fig. 5. Measured distance (blue spot) and accuracy (red) computed as the difference between true (solid black) and measured distance.

In our experiments, the ranging accuracy of the correlation calculation is sensitive to the signal modulation rate and the PSL of the correlation curve which is associated with the correlation symbol length calculated and the system noise. For comparing and analyzing the ranging accuracy, we refer to the optical chaotic system reported in Ref. [21], in which 2 cm accuracy is achieved when SNR (defined as the ratio of the peak amplitude in the correlation trace to three times the standard deviation of the amplitude variations in the background) is higher than

Optics EXPRESS

about 3.8 dB. While, the SNR in the ranging experiment in Fig. 5 maintains at about 3.9 dB. The reason for the difference in the accuracy is that the signal modulation rate and bandwidth of APD we employed are 200 MHz while that of Ref. [21] are 400 MHz. Therefore, by optimizing the transmitting and receiving optics and employing the APD with higher bandwidth and lower noise, we can obtain better ranging accuracy in future research. In addition, because of the limited corridor length in the laboratory, we only tested the distance up to 14 m. This research focuses on initially verifying the feasibility of this ranging system. Actually, the echo signal is still very strong when we measure the distance up to 14 m in the corridor, which means we can test farther distances.

4.2. Anti-interference experiment

To complete the investigation, the anti-interference capability is verified in this section. On the basis of the ranging system established, we investigate the impact of chaotic signals, square wave signals, and sine wave signals interference on our chaotic lidar system. For convenience, the interference signal source is generated by AWG and received by APD on the same optical path. For simulating the same type of lidar, the transmitted power of the interference signal maintains the same as the original system. Furthermore, with the standard board placed at 8 m, we investigate the effect of the modulation rate of the jamming signals at 10 MHz, 100 MHz, 200 MHz and 1 GHz on the anti-interference capability.

With the interference of different waveforms, the cross-correlation results are shown in Fig. 6, which indicates that there is still an apparent peak value on the curve, thus validating the expected anti-interference capability. However, for different interference waveforms and modulation rates, the effects of anti-interference are also different. As shown in Fig. 6(a), without interference, the PSL is −7.29 dB. Firstly, for the chaotic waves interference, the PSL obtained under the interference with modulation rates of 10 MHz, 100 MHz, 200 MHz and 1 GHz are −2.06 dB, −4.45 dB, −6.13 dB, and −7.27 dB respectively. Since the bandwidth of the system is 200 MHz, if the modulation rate of the interference signal is over 200 MHz, the amplitude of the received interference signal will be extremely small, which means that high-frequency signals will be filtered out. Therefore, 1 GHz interference has a slight impact on the PSL. However, as shown in Figs. 6(b)–6(c), due to the bandwidth restriction of the APD we employed, it appears to be so insensitive to the square waves and sine waves interference with 100 MHz and 200 MHz modulation rates where the amplitude of the received interference signal also be reduced and the PSLs remain unchanged basically. By contrast, for 1 MHz interference signal, the amplitude received by APD is relatively high which caused the reduction of PSL. Therefore, For the sake of further investigating and exploring the general regularity, we further explore the relationship between different parameters and the anti-interference effect through simulation which is convenient to control variables.

4.3. Anti-interference analysis and simulation

On the basis of the original 200 MHz chaotic signal in the above experiments, we simulate the interference signals with different modulation rates, waveforms, and signal to interference plus noise ratio (SINR). The sampling rate is 2.5 Gs/s, and the correlation symbol length is 800 (4 μs). With different SINR from 1:1 to 1:5, we investigate the influence of the modulation rate at 500 kHz, 1 MHz, 100 MHz, 200 MHz and 800 MHz of the interference signal on the system cross-correlation effects. As shown in Fig. 7, the PSL is shown to be sensitive to the SINR. When decreasing the SINR, the PSL increases proportionally. From Fig. 7(a), for chaotic wave interference, we can see that the PSL values obtained are higher when the modulation rate of interference signal at 100 MHz and 200 MHz, which indicates the cross-correlation effect is relatively worse. While, Fig. 7(b) shows that the PSL has the highest value at 1 MHz modulation

Optics EXPRESS

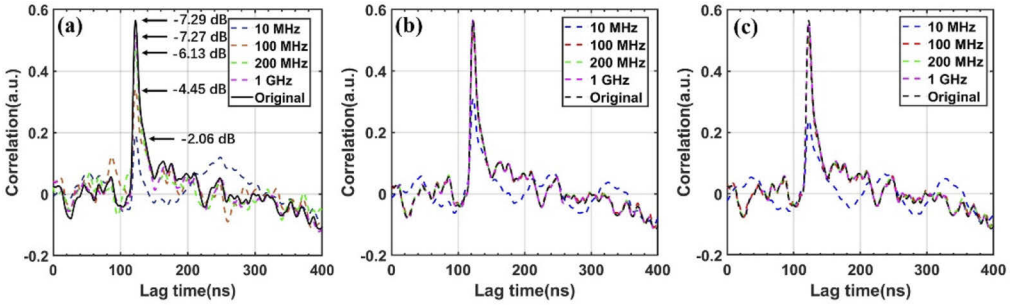

Fig. 6. The cross-correlation results of chaotic signal with the interference of (a) chaotic wave, (b) square wave, (c) sine wave signal at 10 MHz, 100 MHz, 200 MHz and 1 GHz modulation rate.

rate for square wave interference. Besides, in Fig. 7(c), for sine wave interference, the worst case occurs at the same-frequency interference of 200 MHz.

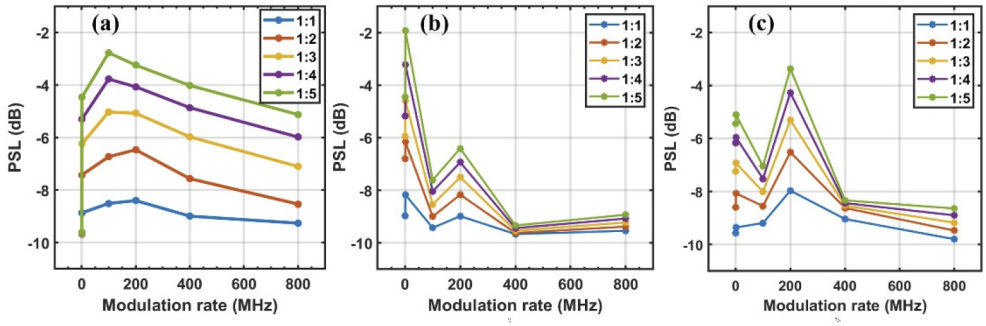

Fig. 7. The PSL of the cross-correlation results of the original 200 MHz chaotic signal with the interference of (a) chaotic wave, (b) square wave, (c) sine wave signal at different modulation rates and SINR.

For the above results, we can analyze the reasons through the interference of square waves. Figures 8(a)–8(f) shows the correlation curves with the square wave interference modulation rate at 250 kHz, 500 kHz, 1 MHz, 10 MHz, 100 MHz and 1GHz when the SINR is 1:3. As shown in Fig. 8(a), for low-frequency interference signals below 250 kHz (4 μs), which means the code length of the interference signal exceeds the correlation length (4 μs), the interference signal has a small influence on the correlation result. From Fig. 8(c), when the ratio of interference code length to the correlation length is 1:4 (1 MHz interference signal), two obvious peaks appear in the side lobes of the correlation curve, resulting in a significant increase in PSL as shown in Fig. 7(b). While, from Figs. 8(d)–8(f), for the high-frequency interference signals, with the increase of modulation rate, the side lobes decreased gradually. Besides, the chaotic wave and the sine wave interference also have similar characteristics. While, the worst situation for the chaotic wave appears at a higher modulation rate due to the aperiodicity of the chaotic wave. For the sine wave, as the single frequency characteristics, the worst situation appears at the same modulation rate of 200 MHz. Therefore, the anti-interference effect can be further improved by reducing the side lobes of the correlation curve in future investigation.

Optics EXPRESS

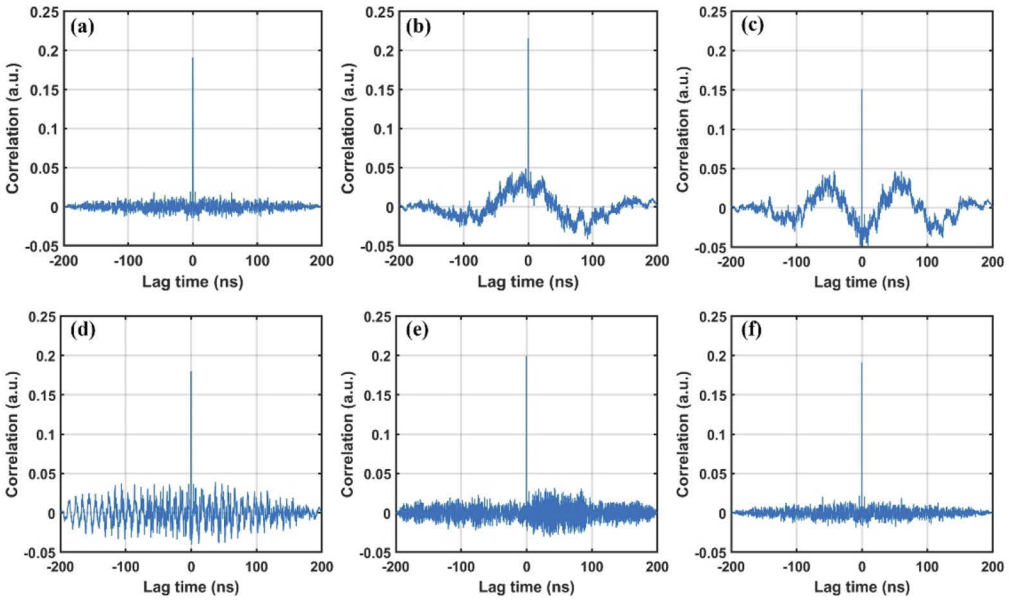

Fig. 8. The correlation curves with the square wave interference modulation rate at (a) 250 kHz, (b) 500 kHz, (c) 1 MHz, (d) 10 MHz, (e) 100 MHz and (f) 1 GHz when the SINR is 1:3.

5. Conclusion

In this study, we establish a digital chaotic lidar system with the chaotic signal generated by FPGA, which is capable of achieving medium-distance detection and high ranging accuracy. It is verified by experiments that it can effectively resist the interference of different waveforms and different frequency signals, and solve the difficulties of complex structure and single modulation mode of an optical chaotic system. We use FPGA to generate random sequences of different modulation rates according to different iterative equations and initial values, and select the initial value 0.7 and improved logistic equation through simulation. Based on this digital chaotic lidar system, centimeter-level ranging accuracy has been successfully achieved. In addition, the chaotic signal, square wave signal, and sine signal generated by the AWG are used as interference sources and simulated as another lidar system, which is received through APD on the optical path. By comparing the experimental results with interference and without interference, the interference of chaotic, square wave, and sine wave signals at modulation rates of 10 MHz, 100 MHz, 200 MHz, and 1 GHz is explored, which demonstrates the significant anti-interference effect of this digital chaotic lidar.

Funding. Special Project for Research and Development in Key areas of Guangdong Province (2018B010114002).

Disclosures. The authors declare that there are no conflicts of interest.

References

1. J. F. Andersen, J. Busck, and H. Heiselberg, "Applications of high resolution laser radar for 3-D multispectral imaging," Proc. SPIE **6214**, 62140U (2006).
2. S. a. Brent, "LIDAR: Mapping the world in 3D," Nat. Photonics **4**(7), 429–430 (2010).
3. F. Moosmann and C. Stiller, "Velodyne SLAM," in *Proceedings of IEEE Conference on Intelligent Vehicles Symposium* (IEEE, 2011), pp. 393–398.
4. Y. Jiang, S. Karpf, and B. Jalali, "Time-stretch LiDAR as a spectrally scanned time-of-flight ranging camera," Nat. Photonics **14**(1), 14–18 (2020).
5. T. Bosch, M. Lescure, R. Myllyla, M. Rioux, and M. C. Amann, "Laser ranging: a critical review of usual techniques for distance measurement," Opt. Eng. **40**(1), 10–19 (2001).

Optics EXPRESS

6. D. Bronzi, Y. Zou, F. Villa, S. Tisa, A. Tosi, and F. Zappa, "Automotive Three-Dimensional Vision Through a Single-Photon Counting SPAD Camera," IEEE Trans. Intell. Transport. Syst. **17**(3), 782–795 (2016).
7. G. Kim, J. Eom, and Y. Park, "Investigation on the occurrence of mutual interference between pulsed terrestrial LIDAR scanners," in *Proceedings of IEEE Conference on Intelligent Vehicles Symposium* (IEEE, 2015), pp. 437–442.
8. M. Hebel, M. Hammer, M. Arens, and A. L. Diehm, "Mitigation of crosstalk effects in multi-LiDAR configurations," Proc. SPIE **10796**, 3 (2018).
9. P. Du, D. Geng, W. Wang, and M. Gong, "Laser detection of remote targets applying chaotic pulse position modulation," Opt. Eng. **54**(11), 114102 (2015).
10. J. Hao, M. L. Gong, P. F. Du, B. J. Lu, F. Zhang, H. T. Zhang, and X. Fu, "Ultra-low power anti-crosstalk collision avoidance light detection and ranging using chaotic pulse position modulation approach," Chin. Phys. B **25**(7), 074207 (2016).
11. C. M. Tsai and Y. C. Liu, "Anti-Interference Single-Photon LiDAR Using Stochastic Pulse Position Modulation," Opt. Lett. **45**(2), 439–442 (2020).
12. J. Riemensberger, A. Lukashchuk, M. Karpov, W. Weng, and T. J. Kippenberg, "Massively parallel coherent laser ranging using a soliton microcomb," Nature **581**(7807), 164–170 (2020).
13. N. Kuse and M. E. Fermann, "Frequency-modulated comb LIDAR," (2019).
14. A. J. Hymans and J. Lait, "Analysis of a frequency-modulated continuous-wave ranging system," in *Proceedings of IEEE Conference on Electronic & Communication Engineering* (IEEE, 1960), pp. 365–372.
15. F. Y. Lin and J. M. Liu, "Ambiguity functions of laser-based chaotic radar," IEEE J. Quantum Electron. **40**(12), 1732–1738 (2004).
16. K. Myneni, T. A. Barr, B. R. Reed, S. D. Pethel, and N. J. Corron, "High-precision ranging using a chaotic laser pulse train," Appl. Phys. Lett. **78**(11), 1496–1498 (2001).
17. F. Y. Lin and J. M. Liu, "Chaotic lidar," IEEE J. Sel. Top. Quantum Electron. **10**(5), 991–997 (2004).
18. B. Wang, Y. Wang, L. Kong, and A. Wang, "Multi-target real-time ranging with chaotic laser radar," Chin. Opt. Lett. **6**(11), 868–870 (2008).
19. W. T. Wu, Y. H. Liao, and F. Y. Lin, "Noise suppressions in synchronized chaos lidars," Opt. Express **18**(25), 26155–26162 (2010).
20. B. Wang, T. Zhao, and H. Wang, "Improvement of signal-to-noise ratio in chaotic laser radar based on algorithm implementation," Chin. Opt. Lett. **10**(5), 052801 (2012).
21. C. Chih-Hao, C. Chih-Ying, C. Jun-Da, P. Da-Kung, T. Kai-Ting, and L. Fan-Yi, "3D pulsed chaos lidar system," Opt. Express **26**(9), 12230–12241 (2018).
22. H. Sheng, Z. Fuhui, D. Yantao, Z. Zhixin, W. Yuhao, and Y. Maosong, "Chaotic Phase-Coded Waveforms with Space-Time Complementary Coding for MIMO Radar Applications," IEEE Access **6**, 30378–30391 (2018).
23. J. Dai, X. Hao, P. Li, Z. Li, and X. Yan, "Antijamming Design and Analysis of a Novel Pulse Compression Radar Signal Based on Radar Identity and Chaotic Encryption," IEEE Access **8**, 5873–5884 (2020).